Applied Ocean Research 126 (2022) 103301

Contents lists available at ScienceDirect

Applied Ocean Research

journal homepage: www.elsevier.com/locate/apor

Computational fluid dynamics predictions of draught and trim variations on ship resistance in confined waters

Ruaraidh Campbell [a], Momchil Terziev [b,*], Tahsin Tezdogan [a], Atilla Incecik [b]

[a] Department of Naval Architecture, Ocean and Marine Engineering, University of Strathclyde, Glasgow, UK
[b] Faculty of Engineering, University of Strathclyde, Glasgow, UK

ARTICLE INFO

Keywords:
CFD
RANS
Shallow water
Trim angle
Draught change

ABSTRACT

Adjusting a vessel's trim and draught to enhance resistance characteristics is a promising strategy to improve the energy efficiency of maritime transport. However, the vast majority of scientific effort has been directed at such gains in deep, unrestricted waters. Shallow and confined waters modify the flow and pressure distribution around a ship, altering considerably the resistance curve. This study aims to elucidate trim and draught increase effects on a ship's resistance while advancing through a restricted waterway using Computational Fluid Dynamics. The results show that increasing the draught of a benchmark hull magnifies the hydrodynamic resistance by approximately 10% to 15% depending on the ship speed. This added hydrodynamic resistance may be compensated by adjusting the vessels' trim, but the ability to compensate the added hydrodynamic resistance is sensitive to ship's speed. At low speeds, the numerical model predicts the increase in resistance due to a 10% higher draught can be reduced by varying the trim angle leaving the total resistance 0.87% higher than at the design draught and zero trim angle condition. On the other hand, higher speeds offer a greater potential for resistance reduction through trim.

1. . Introduction

The area of shallow water hydrodynamics is an important field of study due to the constant increase in increased ship size and speed (Tuck, 1978). Shallow and confined water ship hydrodynamics is an expanding field as ways to safely reduce emissions and costs arising from transport of goods are sought, particularly in coastal and inland waterways. For example, inland waterway transport can be significantly more energy efficient than road transport, reducing congestion, noise, and pollution in coastal cities, or cities near inland waterways. Greater use of transport over water is an effective way to effect substantial emission reduction at local, national, and supranational levels. This has led The European Commission (2020) to devise strategies to realise the potential of waterborne transport and carry out impact assessments.

Shallow and confined water effects must be taken into account for all vessels, since ocean-going ships must enter shallow and narrow waterways each journey. Advancements in technology have resulted accessible numerical modelling techniques which are frequently used to study shallow water hydrodynamics. These developments have allowed for savings in research costs as experimental methods can require more funds and time. However, both methods remain essential as highlighted by the validation presented in the following sections.

While a number of research papers have been published on the topic of shallow and confined water ship hydrodynamics in the context of coastal waters and inland waterways, several unexamined areas remain. Amongst these is the influence of a ship's loading condition on its performance. Research into potential optimisation and energy efficiency improvements in deep water has been carried out by several researchers. For example, Shivachev et al. (2017) performed a numerical and experimental study of the trim influence of a container ship using computational and experimental methods. Sun et al. (2016) created a trim optimisation software and validated their results against full-scale trials. However, the influence of ship trim and draught are not frequently studied in shallow and confined waters.

The main aim of this paper is to investigate the effects of loading condition on the resistance of a vessel sailing in shallow waters. This is done using the commercial CFD software package Star-CCM+, version 14.06.008. For this study, the widely used KCS model is analysed under different draughts and trim angles. The importance of investigations of this nature in recent times has increased drastically due to the formerly discussed constant demand for increase in ship size and speed. The motivation behind this work is to enhance the understanding and

* Corresponding author.
E-mail address: momchil.terziev@strath.ac.uk (M. Terziev).

https://doi.org/10.1016/j.apor.2022.103301
Received 3 March 2022; Received in revised form 3 May 2022; Accepted 26 July 2022
Available online 1 August 2022

Table 1
Ship main particulars.

Parameters	Symbol	Value
Scale	λ	75
Length between perpendiculars (m)	L	3.067
Breadth at water line (m)	B	0.429
Depth (m)	D	0.25
Design draught (m)	T	0.144
Block Coefficient	C_B	0.651

Table 2
Test matrix.

	Trim (°)	Draught increase	Depth-to-draught ratio (h/T)
0.302	−0.9, −0.5, −0.3, 0, 0.3, 0.5, 0.9	0%, 5%, 10%	2.22, 2.12, 2.02
0.4	−0.9, −0.5, −0.3, 0, 0.3, 0.5, 0.9	0%, 5%, 10%	2.22, 2.12, 2.02
0.469	−0.9, −0.5, −0.3, 0, 0.3, 0.5, 0.9	0%, 5%, 10%	2.22, 2.12, 2.02
0.502	−0.9, −0.5, −0.3, 0, 0.3, 0.5, 0.9	0%, 5%, 10%	2.22, 2.12, 2.02
0.57	−0.9, −0.5, −0.3, 0, 0.3, 0.5, 0.9	0%, 5%, 10%	2.22, 2.12, 2.02

knowledge of this topic.

The following sections will first present background on the impact of trim on resistance. This will highlight the practical importance and potential impact of studies such as this. Section 3 will present the methodology used to carry out the CFD simulations for this investigation and explain the numerical setup. Section 4 will first present a validation and verification of a subset of the obtained results, before analysing the full set of case studies. Finally, conclusions and recommendations for future work are given in Section 5.

2. . Background

Sherbaz and Duan (2014) explored the effects of trim on the resistance of the KRISO container ship (KCS) at model scale, finding that a relatively small trim adjustment by stern reduces resistance. They computed a 2.29% reduction in resistance as a result of this adjustment. Later, Du et al. (2017) investigated the effect of varying draught on the performance of the KCS in deep waters using OpenFOAM. They found that the bulbous bow's effectiveness in modifying the bow wave may be compromised depending on the draught. Islam and Soares (2019) modelled the same problem, including varying trim in their test matrix based on the same solver. A significant reduction in ship resistance was predicted to be possible depending on the combination of draught and trim, of approximately 3.9%.

Sun et al. (2016) conducted a combined experimental-numerical study on the resistance of a 4250 TEU container ship. They coupled their CFD model to an optimisation algorithm to compute the response surfaces of the resistance and effective power, finding that each draught and speed showed a different optimum trim. Similar findings were reported by Lyu et al. (2018), who focused on the wave resistance and total resistance, finding a maximum reduction of 26.2% and 7.2%, respectively. Chen et al. (2019) presented a URANS trim optimisation technique based on ordinary Kriging interpolation to reduce resistance of the KCS. They stressed the importance of speed, which their findings suggested change the optimum trim condition. By contrast, Shivachev et al. (2017) predicted that the KCS hull's resistance is always greatest when trimmed by stern across a range of Froude numbers, spanning from 0.18 to 0.26, the latter being the operational speed of the KCS.

More recently, Le et al. (2021) used the US Navy Combatant, DTMB 5415 to investigate the effect of draught and trim on resistance. Their results indicate that savings of 1.5% may be achieved in the total resistance, while the pressure resistance can decrease by up to 8% depending on the case investigated. Around the same time, Wu et al. (2021) used Detached Eddy Simulation to predict the influence of trim on the bow breaking wave generated by the DTMB 5415 hull. They modelled ±1° trim and reported that the breaking wave is influenced considerably by the trim. Trim was found to increase the bow wave

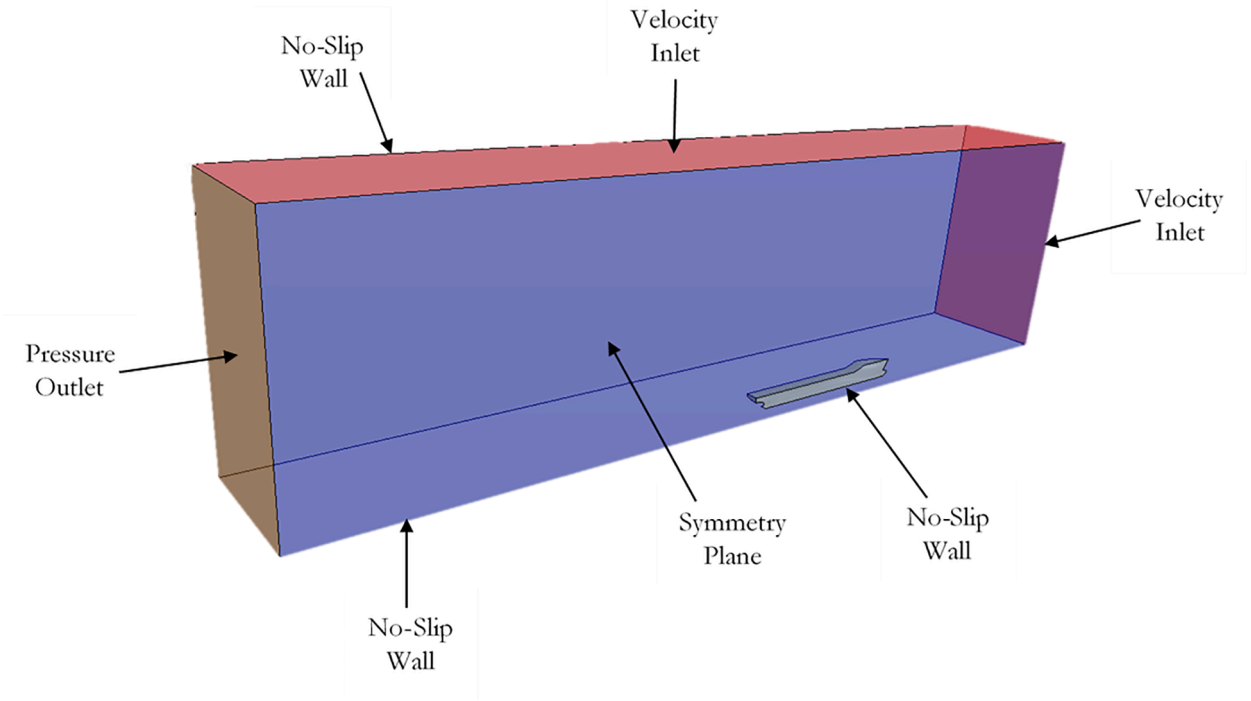

Fig. 1. Computational domain and boundary conditions.

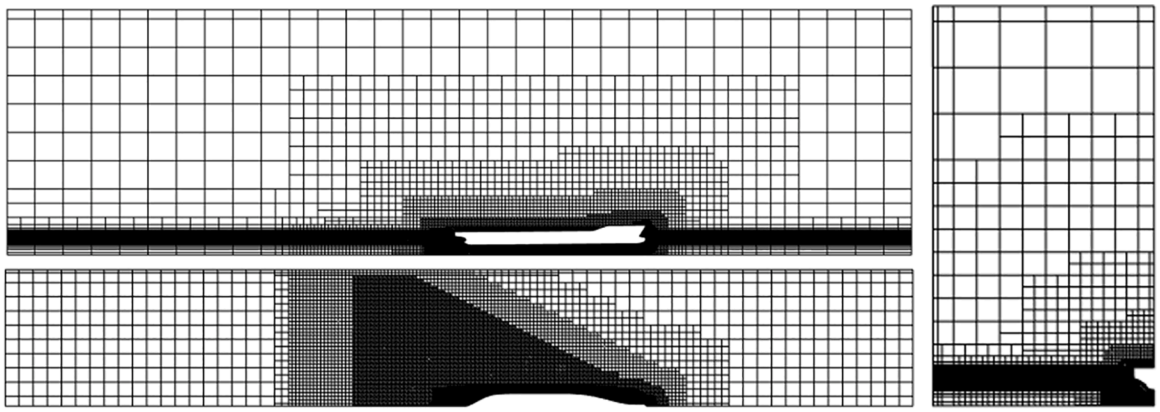

Fig. 2. Three-dimensional view of the computational mesh.

Table 3
Temporal discretisation uncertainty assessment results for the zero trim, 0% draught increase case.

Property	Value				
F_d	0.302	0.4	0.46857	0.502	0.57
Fine (N)	1.29	2.123	2.88	3.35	4.28
Medium (N)	1.3	2.11	2.89	3.33	4.25
Coarse (N)	1.33	2.08	2.89	3.31	4.2
GCI_{time}	0.34%	1.31%	3.44%	1.96%	2.78%

Table 4
Spatial discretisation uncertainty assessment results for the zero trim, 0% draught increase case.

Property	Value				
F_d	0.302	0.4	0.46857	0.502	0.57
Fine (N)	1.29	2.123	2.88	3.35	4.28
Medium (N)	1.32	2.15	2.92	3.29	4.29
Coarse (N)	1.39	2.19	2.95	3.37	4.53
GCI_{mesh}	3.57%	1.64%	3.29%	0.10%	2.41%

Table 5
Validation and verification study results for the zero trim, 0% draught increase case.

Property	Value				
F_d	0.302	0.4	0.46857	0.502	0.57
CFD (N)	1.29	2.123	2.88	3.35	4.28
EFD (N)	1.27	2.28	3.02	3.42	4.47
|% error|	1.64%	7.06%	4.46%	2.08%	4.21%
U_{EFD}	2.20%	2.20%	2.20%	2.20%	2.20%
U_v	4.21%	3.04%	5.24%	2.94%	4.29%
Validated?	**Yes**	**No**	**Yes**	**Yes**	**Yes**
U_{EFD}	0.79%	0.79%	0.79%	0.79%	0.79%
U_v	3.67%	2.24%	4.82%	2.11%	3.77%
Validated?	**Yes**	**No**	**Yes**	**Yes**	**No**

amplitude and resistance, the latter by 4.49%.

Iakovatos et al. (2013) tested the dependence of resistance on trim of six models using CFD. They highlighted the importance of whether the transom is immersed and that resistance is highly sensitive to such changes. The emergence of the bulbous bow was also highlighted as a key factor in determining changes in resistance. Sogihara et al. (2018) investigated how two fine hulls can be trimmed to improve their energy efficiency. They performed self-propulsion experiments on these hulls to determine changes in propulsive power requirements and the components of resistance causing these changes. As reported in previously mentioned studies, the wave component of resistance was responsible for the observed differences and is the component that may be optimised. On the other hand, frictional resistance changes were proportional to the wetted surface area.

As demonstrated above, several authors pointed out that wave resistance changes account for the main changes in vessel performance under different trim and draught conditions. This motivated Park et al. (2015) to combine an investigation of retrofitting alternative bulbous bow forms while varying the ship loading condition leading to changes in the trim and draught. Their CFD model predicted the greatest reduction in resistance of 3% in slow steaming conditions, while the design speed resistance was predicted to reduce by no more than 1%. On the other hand, Moustafa et al. (2015) linked observed changes in resistance as a result of trim and draught variation to the waterline length, showing that improvements in performance are generally achieved when the waterline is smaller.

Findings from the above-mentioned studies can be summarised as follows. Trim can have a significant influence on the resistance of a vessel in calm waters (Altosole et al., 2016) and can therefore be used to improve the energy efficiency of ships (Perera et al., 2015). The frictional resistance of a ship changes relatively little as a result of a varying trim angle (Duan et al., 2019), and is predominantly thought to stem from the change in wetted surface area of the vessel. Since the computational requirements of potential flow approaches are smaller than approaches based on the Navier-Stokes equations, potential flow can be used to assess a large number of cases in an efficient manner (Lv et al., 2013; Lyu et al., 2018). To the best of the authors' knowledge, no previous study has been conducted on the impact of trim and draught on the resistance of a vessel in confined water using CFD. The present paper aims to address this gap in the literature.

3. Numerical modelling and case studies

This section will provide details of the main steps in setting up the numerical investigation and how the results were obtained along with the adopted case studies. The averaged continuity and momentum equations in tensor form and Cartesian coordinates can be written as follows (Ferziger and Peric, 2002):

$$\frac{\partial(\rho\overline{u}_i)}{\partial x_i} = 0 \tag{1}$$

$$\frac{\partial(\rho\overline{u}_i)}{\partial t} + \frac{\partial}{\partial x_j}\left(\rho\overline{u}_i\overline{u}_j + \rho\overline{u'_i u'_j}\right) = \frac{\partial\overline{p}}{\partial x_i} + \frac{\partial\overline{\tau}_{ij}}{\partial x_j} \tag{2}$$

Where $\overline{\tau}_{ij}$ is the mean viscous stress tensor component, expressed by:

$$\overline{\tau}_{ij} = \mu\left(\frac{\partial\overline{u}_i}{\partial x_j} + \frac{\partial\overline{u}_j}{\partial x_i}\right) \tag{3}$$

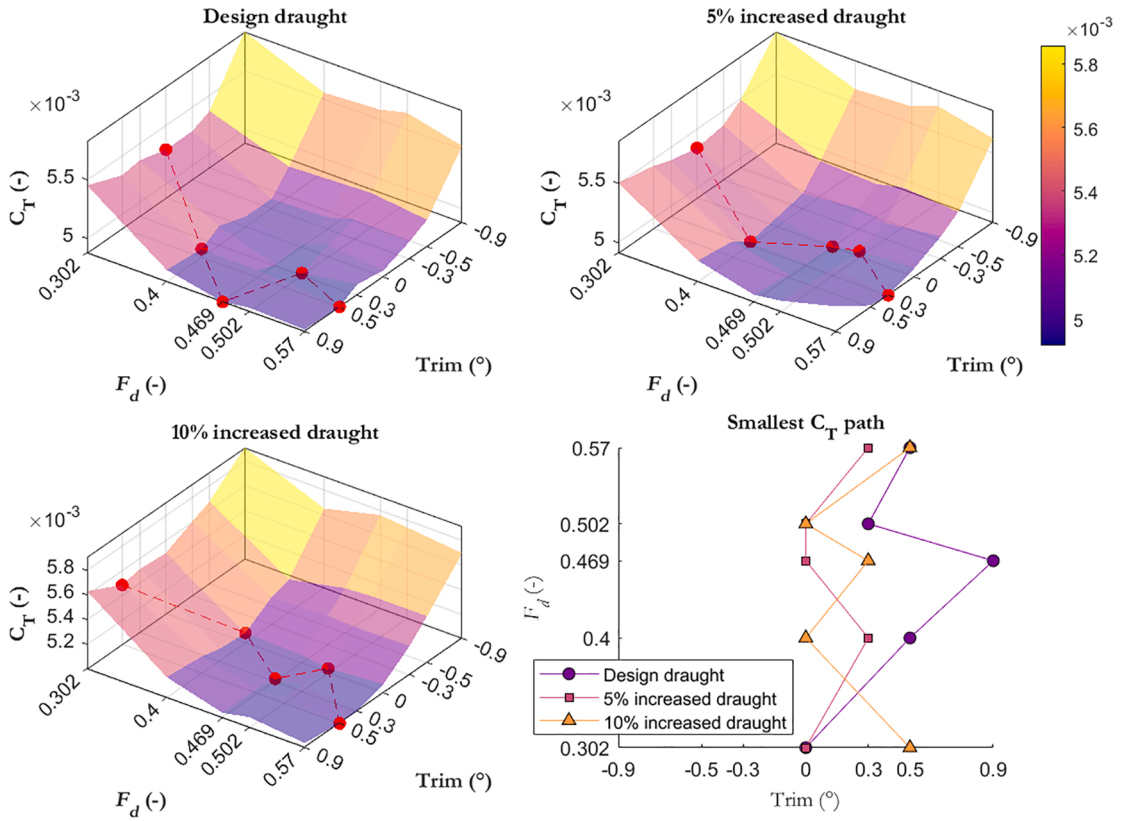

Fig. 3. Total resistance coefficients. The red lines indicate the least total resistance coefficient achieved at each speed. These are given in the bottom right tile of the figure for each trim and draught condition.

In Eqs. (1)–(3), p is the mean pressure, $\overline{u}_i$ is the averaged Cartesian component of velocity, and $\rho\overline{u}_i\overline{u}_j$ is the Reynolds stress.

3.1. Ship particulars and channel geometry

The KRISO Container Ship (KCS) model is used in this study following Elsherbiny et al. (2019b, 2019a) against whose experimental results the present CFD model is validated. There is a large number of readily available data for this model as well as many different studies which adopt the KCS geometry. The main particulars are given below in Table 1. It should be noted that no full-scale ship exists.

The KCS is modelled in a scale of λ=75, matching the experimental work of Elsherbiny et al. (2019b, 2019a) to avoid any scale effects. The water depth in the aforementioned study was $h = 0.32$ m, corresponding to a depth-to-draught ratio of 2.22, and the width of the waterway was 4.6 m with the ship sailing along the centreline. While the experiment featured a number of speeds, attention is focused on the range $0.3 < F_d < 0.57$ in the present work, split into five F_d values, as shown in Table 2. Here, $F_d = V/\sqrt{(gh)}$ is the depth Froude number, expressing the ratio of the ship and wave speed; g is the gravitational acceleration. For each depth Froude number, three draughts and nine trim angles are modelled. These include a 5% and 10% increase in ship draught, and a 0°, ±0.3°, ±0.5°, and ±0.9° trim, where trim by bow is positive. The full test matrix is given in Table 2.

The ratio between a vessel's draught and the waterway depth is a key parameter determining the relative importance of shallow water effects on ship performance. Smaller underkeel clearances magnify the shallow water effect on ship resistance. For this reason, in the present assessment the KCS design draught is increased as stated earlier, reducing the available underkeel clearance. Increasing a vessel's draught is also a strategy to improve energy efficiency of inland craft, suggested by the IWA (Inland Waterways Association, 2020) since this allows the fitting of a larger diameter propeller. However, the hydrodynamic consequences of such a modification must be examined to determine the added drag as a result of the increase in wetted area. The KCS is chosen for this assessment because of the wealth of results available, in fact, a significant minority of the literature cited in the previous section uses the KCS to conduct investigations.

3.2. Computational domain and boundary conditions

The computational domain was modelled in half as the resistance problem is symmetrical. Fig. 1 gives a 3D view of the domain used in Star-CCM+. The boundary conditions were selected based on ITTC (2011) recommendations. Specifically, the velocity inlet is placed 1.5 ship lengths upstream of the forward perpendicular, while the pressure outlet is positioned 2.5 ship lengths downstream of the aft perpendicular. The pressure outlet boundary condition prevents backflow. Moreover, it is possible to set a constant pressure, equal to the hydrostatic pressure, accelerating convergence. The top boundary is a velocity inlet, placed 1.25 ship lengths above the mean waterline.

The choice of boundary conditions can have a relatively small effect on ship resistance when a boundary is located far from the region of interest, in this case, the ship hull. However, in shallow and restricted water conditions, one has limited freedom to position the domain boundaries, since the dimensions of the computational domain must conform to the experiment. As stated previously, for the simulations carried out in this study, the half width is 2.3 m and the water depth is 0.32 m (Elsherbiny et al., 2019b). The only boundary with few restrictions imposed is the top, which is set as a velocity inlet because so-called open boundaries accelerate the solver's convergence properties. A flow velocity equal to the free stream is set in the negative x direction only, mimicking a domain extending infinitely in the z direction. The side and bottom boundaries are set as no-slip walls to conform to the experimental set-up.

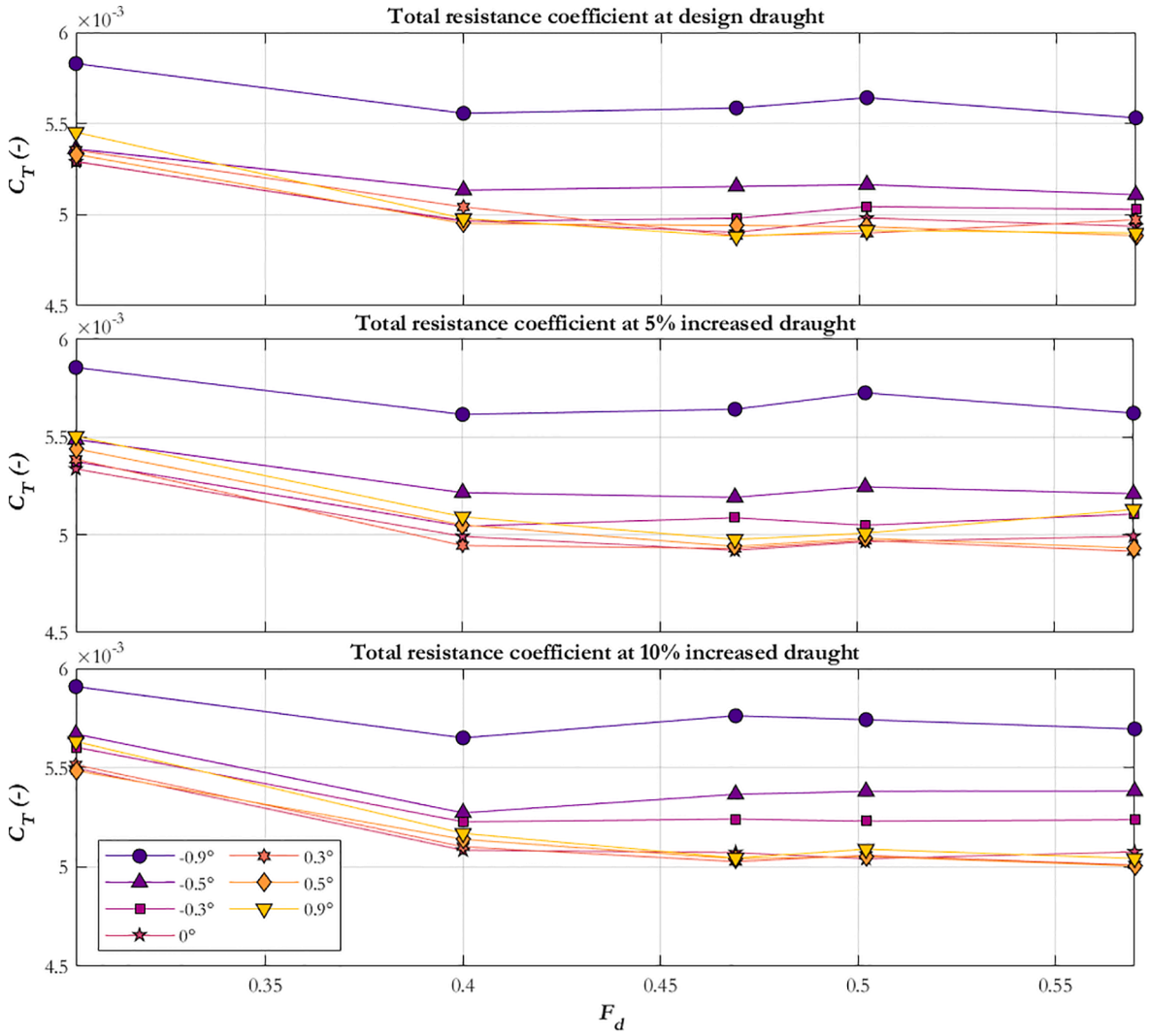

Fig. 4. Total resistance coefficient against depth Froude number at each draught and trim angle.

3.3. Physics modelling

In order to model the fluid flow, Star CCM+ uses the finite volume method, where the integral form of the conservation equations is used and the domain is divided into a finite number of control volumes (Siemens, 2018).

In this study the Realizable k-ε turbulence model was selected. This model is used in similar studies (Tezdogan et al., 2016) as it gives a good agreement with experimental data. Terziev et al. (2020b) carried out a study to investigate the differences between turbulence models in CFD simulations. In comparing the resistance, sinkage and trim results obtained with each model to experimental results, it was found that the average error for the k-ε model was 2.48%. The average between all methods was 3.13%, meaning that the k-ε model provided reasonable results.

The volume of fluid (VOF) method was applied to model the free surface in all numerical simulations. To accelerate convergence of the results, the VOF wave damping function was applied with a value of 2 m on the inlet and outlet. This was applied to the aforementioned inlet and outlet ends of the domain only to allow possible reflections from the side of the canal geometry.

Terziev et al. (2020b) stated the importance of the chosen convection scheme. In this study's CFD work a 2nd order convection scheme was used as it is known that changing this to 1st order causes a loss of accuracy (Andrun et al., 2018). A segregated flow model was applied to the CFD simulations. This allows the RANS solver to solve the flow equations in an uncoupled manner using the Semi-implicit Method for Pressure Linked Equations (SIMPLE) algorithm.

In this work, the ship model was not allowed to sink or trim in the numerical towing tank to isolate the effects of resistance change resulting from the loading condition. Modelling ship squat increases the computational requirements. For example, the impulsive start of the ship creates long waves which require time to eliminate even with wave damping imposed on the inlet and outlet boundaries. These waves amplify unsteadiness created by ship sinkage and trim. The combination of these facts increases the physical time the simulation must run for, as well as the time per iteration. To ensure ship squat effects do not skew the results presented in the following section by an unacceptable margin, a validation and verification study is performed. Validating the numerical model ensures that the error introduced by the neglect of ships squat is tolerable. A similar approach has been adopted in a number of studies (Du et al., 2020; Le et al., 2021; Pacuraru and Domnisoru, 2017; Rotteveel et al., 2017).

3.4. Time step and stopping criteria

Tezdogan et al. (2016) discussed two approaches when it comes to selecting the time step. The first is proposed by ITTC (2014), which recommends a time step value for resistance predictions based on Eq. (4).

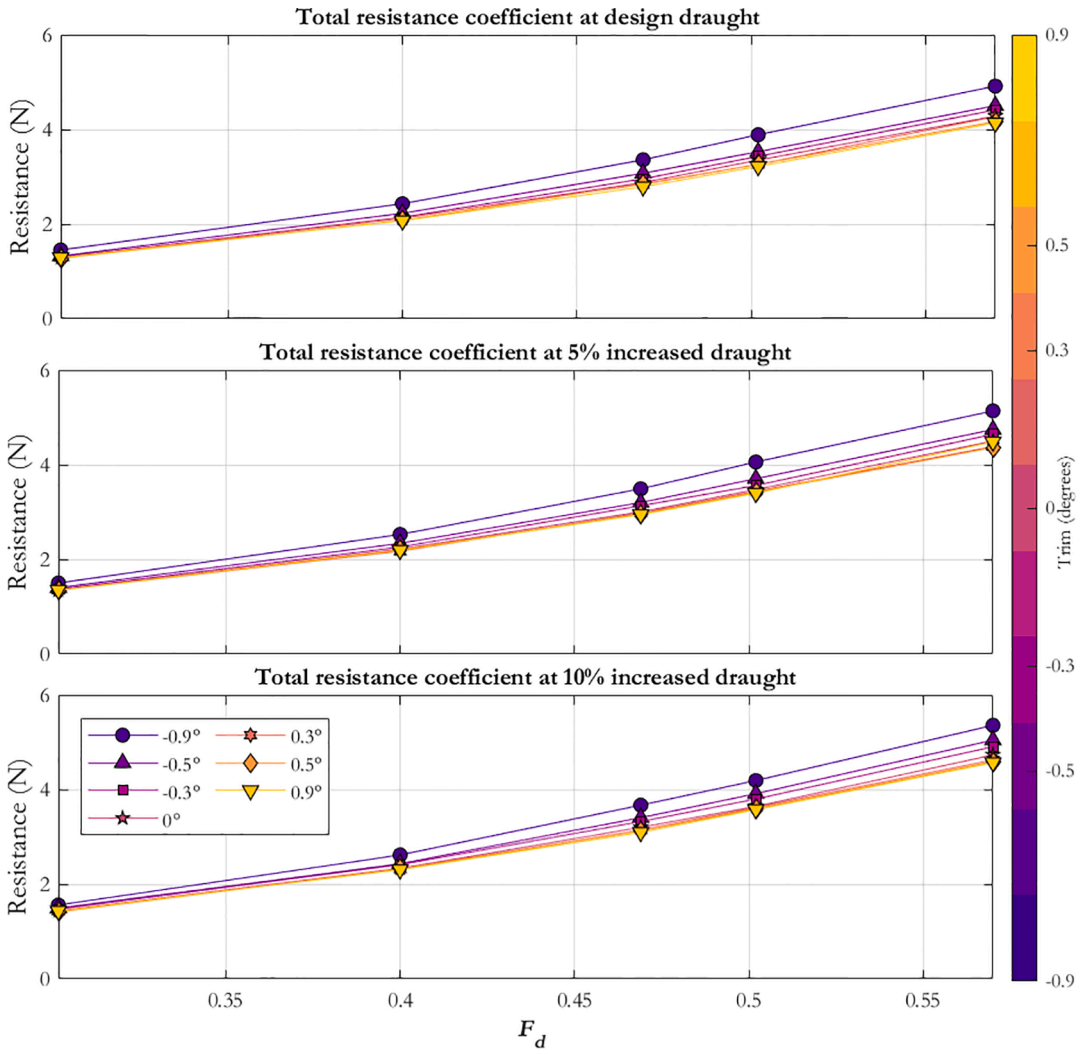

Fig. 5. Total resistance against depth Froude number.

$$\Delta t = 0.005 \sim 0.01L/V \tag{4}$$

where L is the ship length in metres. However, a convergence study carried out by Tezdogan et al. (2016) found that a much smaller time step would be more suitable. Therefore, Eq. (5) was used to calculate the time step for this study:

$$\Delta t = 0.0035L/V \tag{5}$$

Each simulation was allowed to run for a maximum of 200 s which was sufficient for convergence without requiring unreasonable CPU time demands. The time step is advanced at the end of 10 inner iterations. This approach was found to reduce residuals by between 3 and 4 orders of magnitude. Finally, a first order temporal discretisation was used for the unsteady term in the governing equations. All other discretisation terms are set to second order accuracy.

3.5. Mesh generation

Star CCM+ provides automatic meshing tools for generating a mesh, which were applied in this study. As is the case in Tezdogan et al. (2016) a trimmed cell mesher was applied with hexahedral cells. Jones and Clarke (2010) stated that selecting tetrahedral cells can cause a loss of accuracy in the solution which motivated the choice of hexahedral cells.

The mesh settings around the area of the hull and also the expected ship wake were focused on to ensure the more complex flow around these areas was solved accurately. The areas of refinement corresponding to the Kelvin wedge were achieved using custom refinements. The prism layer mesher was used to create near-wall cells at the ship. Values of y^+ between 30 and 100 were maintained throughout.

Fig. 2 depicts a three-dimensional view of the computational mesh. It should be noted that the mesh shown in Fig. 2 does not change significantly when varying the trim and draught of the vessel. The total cell numbers for the level keel condition were approximately 1.05 million, while the remaining cases, with small variation of circa 1000 cells caused by changing the draught/trim. Hereafter, the condition in which the vessel has a trim of 0° is referred to as the level keel condition.

4. Results and discussion

This section will analyse and discuss the results obtained from the CFD simulations, starting with a validation and verification study.

4.1. Validation and verification

This section presents a validation and verification study. Any numerical solution relying upon the mapping of partial differential equations onto discrete notes or time-intervals inevitably induces errors (Terziev et al., 2020a). There are a number of methods to estimate these errors and corresponding uncertainty. Some rely on an error transport equation (Phillips, 2014; Yan and Ollivier-Gooch, 2017), others employ

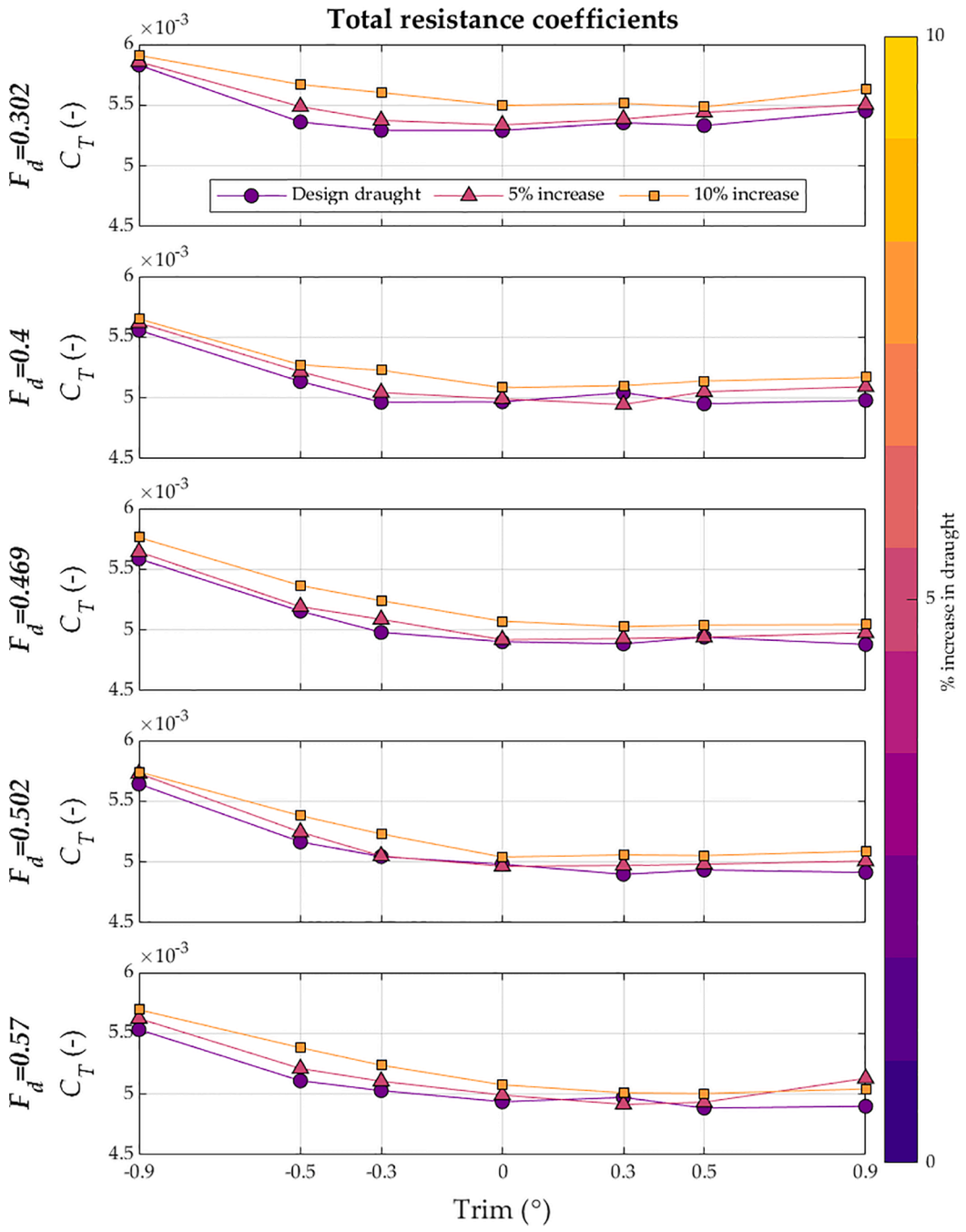

Fig. 6. Total resistance coefficients against trim angle.

a priori techniques based on the mesh (Kallinderis and Kontzialis, 2009). By far the most popular approach and arguably the simplest is the *a posteriori* method based on Richardson Extrapolation (RE) (Richardson, 1927). This technique relies on solving additional numerical simulations with different mesh/time step densities to predict the behaviour of the solution with respect to the asymptotic limit. The procedure begins by coarsening the mesh or time step by a (in this case) constant factor, referred to as the mesh refinement factor, $\boldsymbol{r}$, chosen as $\boldsymbol{r} = \sqrt{2}$ in line with recommendations from the open literature (ASME (American Society of Mechanical Engineers), 2009; ITTC, 2017).

The fine ($\boldsymbol{S}_1$) mesh and time step are coarsened twice to produce the medium ($\boldsymbol{S}_2$) and coarse ($\boldsymbol{S}_3$) solutions. While changing one parameter, all other settings are maintained the same. For example, when magnifying the time step, the mesh is copied. Once the medium and coarse solutions are obtained, the differences between the medium and fine ($\boldsymbol{\varepsilon}_{21} = \boldsymbol{S}_2 - \boldsymbol{S}_1$) and coarse and medium ($\boldsymbol{\varepsilon}_{32} = \boldsymbol{S}_3 - \boldsymbol{S}_2$) are used to predict the convergence ratio ($\boldsymbol{R}$), shown in Eq. (6).

$$R = \varepsilon_{21}/\varepsilon_{32} \tag{6}$$

The convergence ratio determines the type of convergence or divergence observed. When $0 < R < 1$, monotonic convergence is achieved; when $R < 0$, $|R| < 1$, oscillatory convergence is observed. All other cases result to divergence, whether oscillatory ($R\langle 0,\ |R|\rangle 1$) or monotonic ($R > 1$). The inverse of R is used to predict the observed order of accuracy (p) as given by Celik et al. (2008):

$$p = \left|\ln\left|\frac{\varepsilon_{32}}{\varepsilon_{21}}\right| + q(p)\right| \times 1 \Big/ \ln(r_{21}) \tag{7}$$

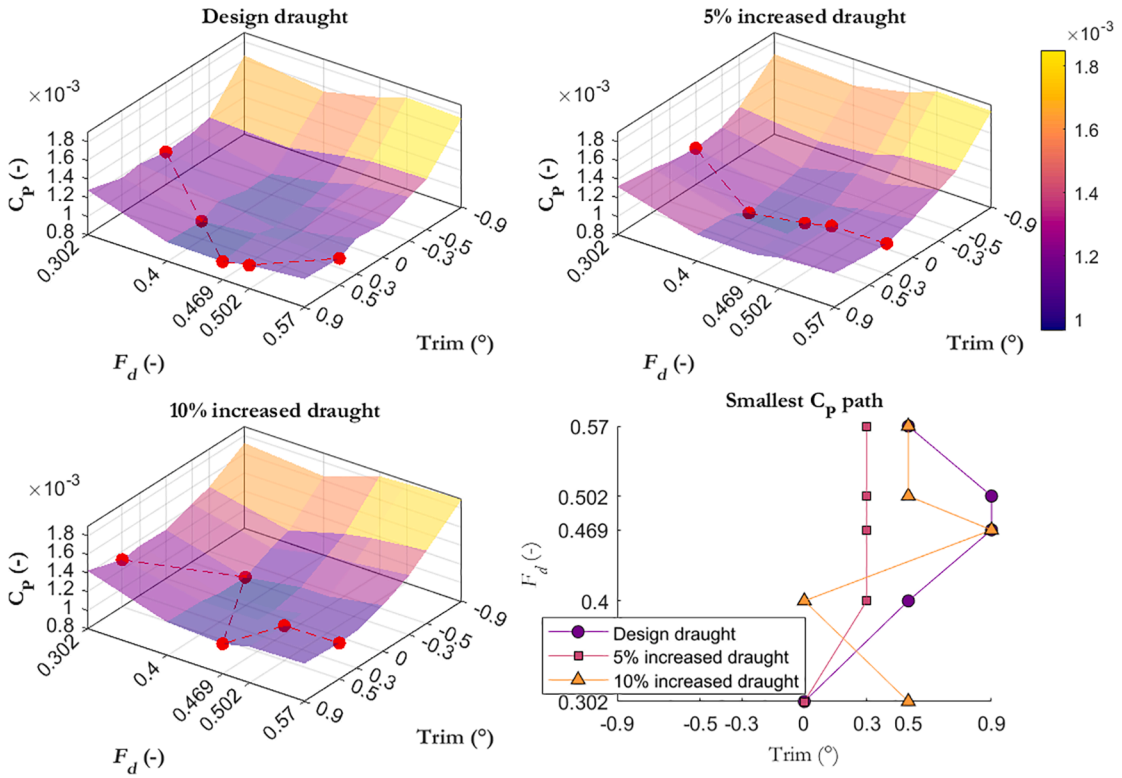

Fig. 7. Pressure resistance coefficients. The red lines indicate the least total resistance coefficient achieved at each speed. These are given in the bottom right tile of the figure for each trim and draught condition.

where $q(p) = 0$ since the refinement ratio between the medium (r_{21}) and coarse (r_{32}) solutions is kept constant, $r_{21} = r_{32} = r = \sqrt{2}$. The cell numbers used in the medium (S_2) mesh case were 547,028, while the coarse (S_3) simulation contained 281,686 cells. The time step is varied by multiplying Eq. (5) by r and r^2 to obtain the medium (S_2) and coarse (S_3) case, respectively. Once the order of accuracy is known, the Grid Convergence Index (GCI), based on the work of Roache (1998) can be estimated as shown in Eq. (8).

$$GCI = 100 \times \left| \frac{1.25(S_1 - S_2)}{S_1(r^p - 1)} \right| \tag{8}$$

The GCI value represents a symmetrical band around the fine solution indicating the uncertainty due to the choice of time step or mesh based on the coarsened parameter. For the purposes of this study, the total resistance of the vessel is used as the studied parameter. The multiplicative value of 1.25, known as the Factor of Safety, is necessary to bring the confidence interval of the GCI prediction to 95%, whereas standard RE has a coverage of only 50%. The GCI values for the time and space-induced discretisation uncertainty and error are shown in Table 3 and Table 4, respectively.

Once the GCI values for each of the aforementioned parameters is known, the validation uncertainty, U_V can be estimated as shown in Eq. (9).

$$U_V = \sqrt{GCI_{mesh}^2 + GCI_{time}^2 + U_{EFD}^2} \tag{9}$$

where U_{EFD} is the experimental uncertainty. According to Elsherbiny et al. (2019b), the uncertainty for low speeds is 2.2% for resistance. On the other hand, for high speeds, the experimental uncertainty is 0.79%. Elsherbiny et al. (2019b) do not specify a definite speed past which the high-speed uncertainty should be taken. For this reason, both cases (with $U_{EFD} = 2.2\%$, and $U_{EFD} = 0.79\%$) are compared in the validation and verification exercise in Table 5. It should be noted that iterative uncertainties were checked prior to conducting the validation exercise using the method of Roy and Blottner (2006) and were in the region of 10^{-4}%. A simulation is considered validated when the validation uncertainty, derived using Eq. (9) is smaller than the error between the fine solution (S_1) and experimental (EFD) value (where the error is defined as $|\%\ \text{error}| = |(CFD - EFD)/EFD| \times 100$).

Table 5 contains the validation and verification results for all speeds in the case when the ship is operating at its design draught and with a 0° trim angle. It should be noted that in the experiment of Elsherbiny et al. (2019b), the ship is allowed to sink and trim, whereas in the current numerical model, the ship is fixed. According to the validation and verification results given in Table 5, all speeds except $F_d = 0.4$ are validated when assuming the low speed experimental uncertainty ($U_{EFD} = 2.2\%$) is valid. On the other hand, when the high speed uncertainty value of $U_{EFD} = 0.79\%$ is taken as valid, the cases when $F_d = 0.4$ and $F_d = 0.57$ are not validated. When the ship speed corresponds to $F_d = 0.4$, the comparison error is approximately 7.06%, the highest of all cases, whereas the validation uncertainties are 3.04% and 2.24% for the low and high speed cases, respectively.

The validation uncertainties (U_V, predicted as shown in Eq. (7)), are predicted in the range 2.94% to 5.24% in the low speed U_{EFD} cases corresponding to $F_d = 0.502$, and $F_d = 0.469$, respectively. On the other hand, the high speed validation uncertainties, that is, when the experimental uncertainty is taken as the lower value of 0.79%, U_V values range between 2.11% and 4.82% for $F_d = 0.502$, and $F_d = 0.469$, respectively.

Since the validation uncertainties comprise grid and time step-induced uncertainties, it is instructive to examine which parameter attains greater values for each speed. Doing so presents a mixed picture:

- For the two lowest speeds ($F_d = 0.302$, and $F_d = 0.4$) the time step is responsible for greater numerical uncertainty. However, the magnitude to the GCI uncertainty decreases as the speed is increased from $F_d = 0.302$ to $F_d = 0.4$ by up to one half.

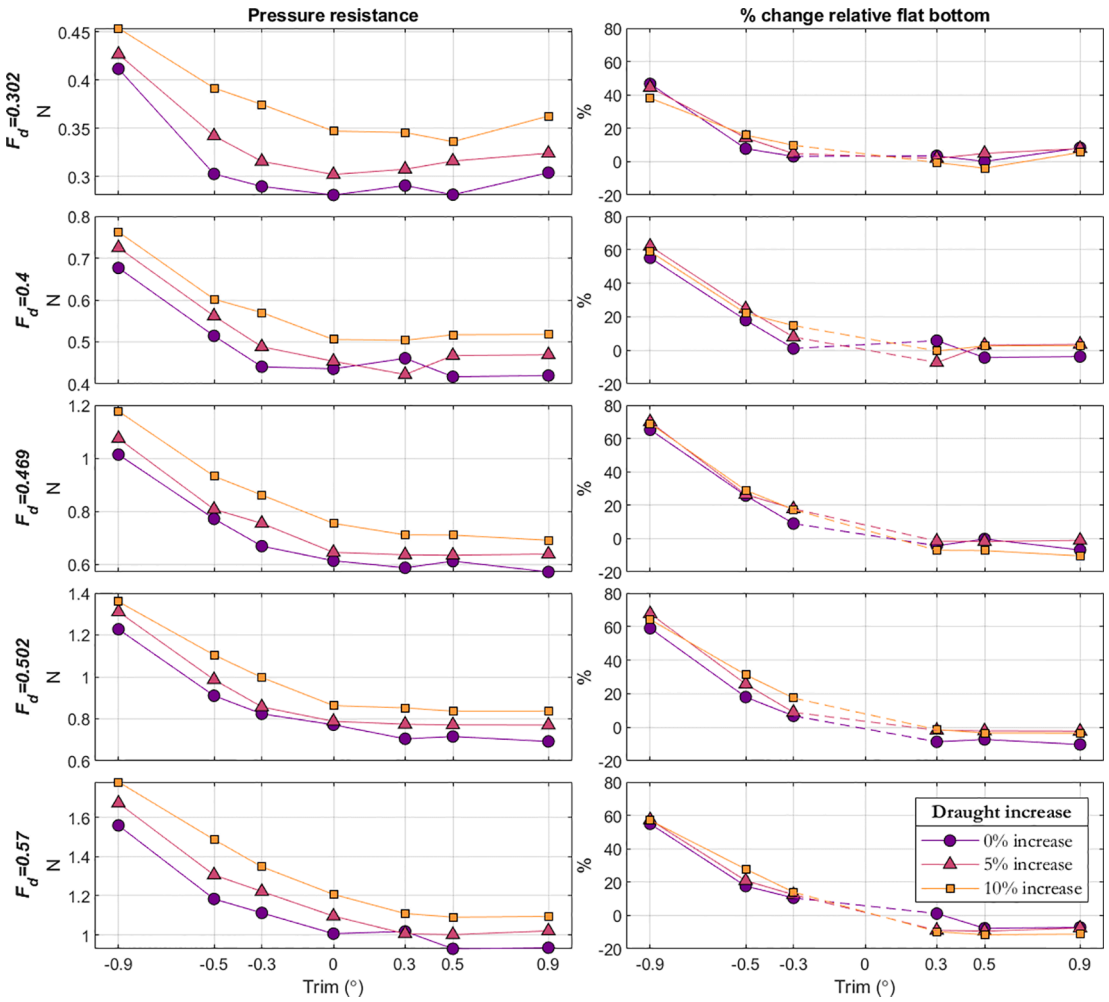

Fig. 8. Pressure resistance variation with draught and trim angle.

- For all other speeds, grid dependence is greater than time dependence. This suggests that the manner of setting the time step (Eq. (3)) is relatively effective in maintaining a stable solution in terms of temporal discretisation.

The results of the validation and verification study can be summarised as follows. While the majority of cases were validated, validation was not achieved in some cases (four out of five speeds were validated when $U_{EFD} = 2.2\%$ and three out of five speeds were validated when $U_{EFD} = 0.79\%$). However, since the majority were validated regardless of the experimental uncertainty, the validation and verification exercise is considered successful. Discretisation uncertainties were found to be within tolerable levels, with no case exceeding 3.44% (observed for $F_d = 0.469$) when performing grid coarsening, and 3.57% (observed for $F_d = 0.302$) when studying the influence of the time step. It should be noted that the uncertainties reported within this section are assumed to hold for all other cases mentioned in Table 2.

4.2. Resistance results for varying trim angle and draught

This section contains the computed resistance coefficients for all cases, including variations in depth Froude number, trim angle, and draught. Resistance coefficients are computed by dividing the force measured by $0.5\rho SV^2$, where $\rho = 997.561$ kg/m^3 is the fresh water density, S is the submerged area of the hull, measured at each draught and trim angle, and V is the ship velocity. The CFD model decomposes the total resistance into a frictional and a pressure component. In converting these forces to coefficient form, one arrives at the total resistance coefficient (C_T), the pressure resistance coefficient (C_P), and the frictional resistance coefficient (C_F).

Fig. 3 indicates that the total resistance coefficient is influenced considerably by the trim angle. Moreover, the least resistance changes with speed, but trim by bow is more likely to be a favourable condition than trim by stern. This conclusion can be arrived at by examining the bottom right tile of Fig. 3, which shows how each draught and Froude number influence the relative location of the smallest total resistance coefficient measured numerically.

The presence of speed dependence implies an interaction between the effect of changes in the waterline as a result of varying trim and draught, and the resistance hump caused by variations in the wave resistance. To examine such effects, a comparison of the total resistance coefficients against depth Froude number is necessary. This is given in Fig. 4, where the effect of trim is clearly visible. While there is some clustering of the total resistance coefficients when the vessel is trimmed by bow (positive angles), it is evident that trim by stern (negative angles) is unfavourable.

The case where the vessel is modelled with a trim of -0.9° (trim by stern) exhibits the highest resistance coefficients for all depth Froude numbers and draughts. On the other hand, the numerical model predicts that a small trim angle by bow, typically 0.3°~0.5°, is the most favourable of the examined cases. It should be noted that for optima to be identified, the results should have a higher resolution, both with respect to speed, as well as with respect to trim. The resistance coefficients shown in Fig. 4 were computed with the wetted surface area

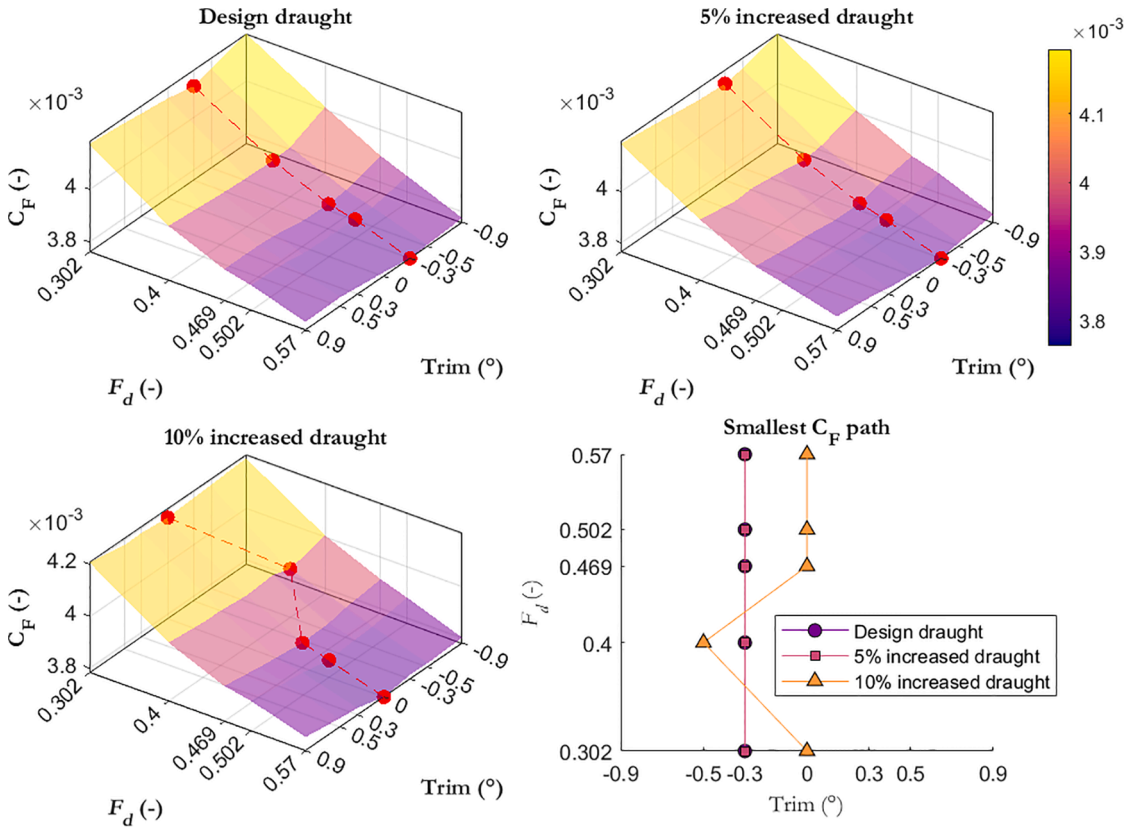

Fig. 9. Frictional resistance coefficients. The red lines indicate the least total resistance coefficient achieved at each speed. These are given in the bottom right tile of the figure for each trim and draught condition.

measured in each case (draught and trim) as mentioned previously. Therefore, these results include the effects of varying submerged wetted surface. It is instructive to examine the dimensional total resistance against depth Froude number to better understand if the hydrodynamic penalty incurred by increasing the draught of the vessel may be negated through trim optimisation. This is shown in Fig. 5, which demonstrates the increase in resistance across all speeds and draughts caused by a negative trim angle (trim by stern).

The total resistance change between trim angles tends to increase at higher speeds indicating a greater potential for savings the higher the speed is. Fig. 5 shows that it is possible to reduce the total resistance by trim optimisation sufficiently to counter the hydrodynamic penalty incurred by draught changes. However, as discussed above, the optimum trim will vary depending on the draught. For example, when the draught is increased by 5%, the least resistance is recorded when the vessel is trimmed by 0.5° The total resistance coefficients for each trim angle are depicted in Fig. 6, where the aforementioned offset can be observed.

As stated earlier, an increase in the draught can be used to fit a larger propeller, thereby increasing efficiency (IWA, 2020). It is therefore important to test the relative impact of draught increases. Draught changes can incur a hydrodynamic penalty in two ways. Firstly, the submerged surface area of the hull changes, therefore, the frictional resistance will be magnified, and secondly, by modifying the flow in the vicinity of the hull and waterline shape leading to differences in pressure resistance.

The literature review section discussed which components of resistance are affected by differences in trim, finding that wave resistance, a component of the pressure resistance, is more sensitive to trim optimisation. In confined waters, although pressure resistance tends to attain a relatively small value, it is of higher importance than in deep, unrestricted waters. It is important to quantify the pressure resistance magnitude to understand changes in the waterline shape which are known to have a great effect on the wavemaking resistance of a hull (Moustafa et al., 2015). Such changes occur due to both trim and draught changes, and may be particularly important if a hull is not operating at the design waterline.

To provide further evidence on the impact of trim and draught changes on the resistance of the hull, it is necessary to examine the generated results for each depth Froude number separately. This is presented in Fig. 6, which confirms the observation made earlier; namely, the highest total resistance coefficient is always the case where the vessel is modelled with a trim of − 0.9° More importantly, Fig. 6 shows that if a vessel is trimmed appropriately, the induced hydrodynamic penalty induced by increasing the draught can be partially offset.

For example, in the even keel case, the total resistance coefficient is approximately 10.68% higher when comparing the design draught and the 10% increased draught cases for $F_d = 0.303$. This difference increases to 15.08% for $F_d = 0.469$ – the highest difference for all speeds. However, the results show that for $F_d = 0.303$, the resistance is only 0.87% higher if the vessel is trimmed by 0.9° For $F_d = 0.57$, the total resistance coefficient may even be lower for the 10% increased draught case than the design draught by 0.34%. This is a result that indicates the importance of calibrating against speed as well as trim and draught.

At this stage, it is convenient to introduce the obtained results for each resistance coefficient. To begin with, the pressure resistance coefficient is given in. The pressure resistance coefficients, given in Fig. 7, represent the normal component of the total drag and contain wave resistance as well as viscous pressure resistance. The data in Fig. 7 show that the pressure resistance is affected to a greater extent by the change in trim rather than speed. The highest C_P values are always observed when the vessel is trimmed by stern (− 0.9°). This explains the preference of the total resistance results towards the positive trim angles, i.e. trim by bow.

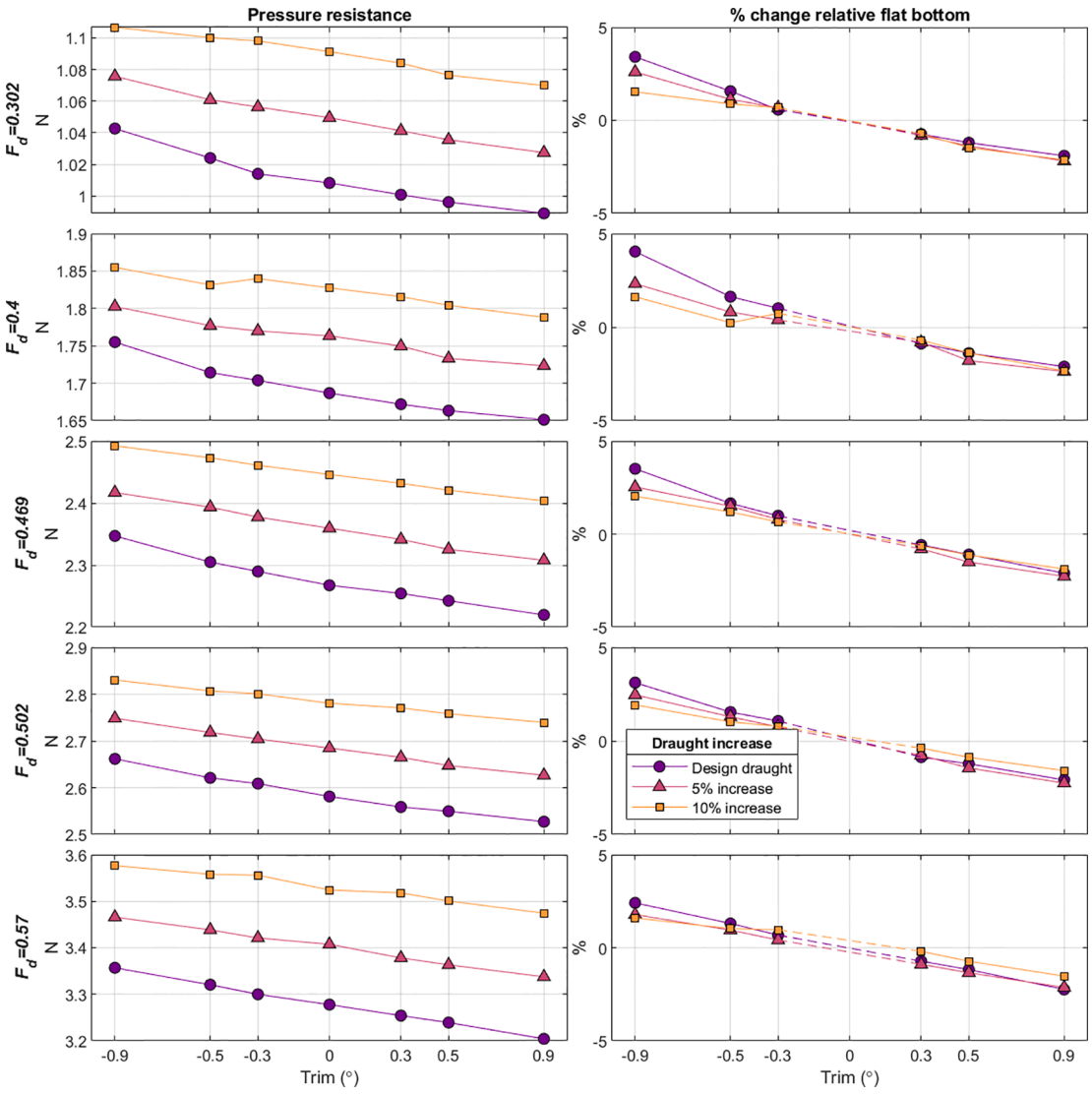

Fig. 10. Frictional resistance variation with draught and trim angle.

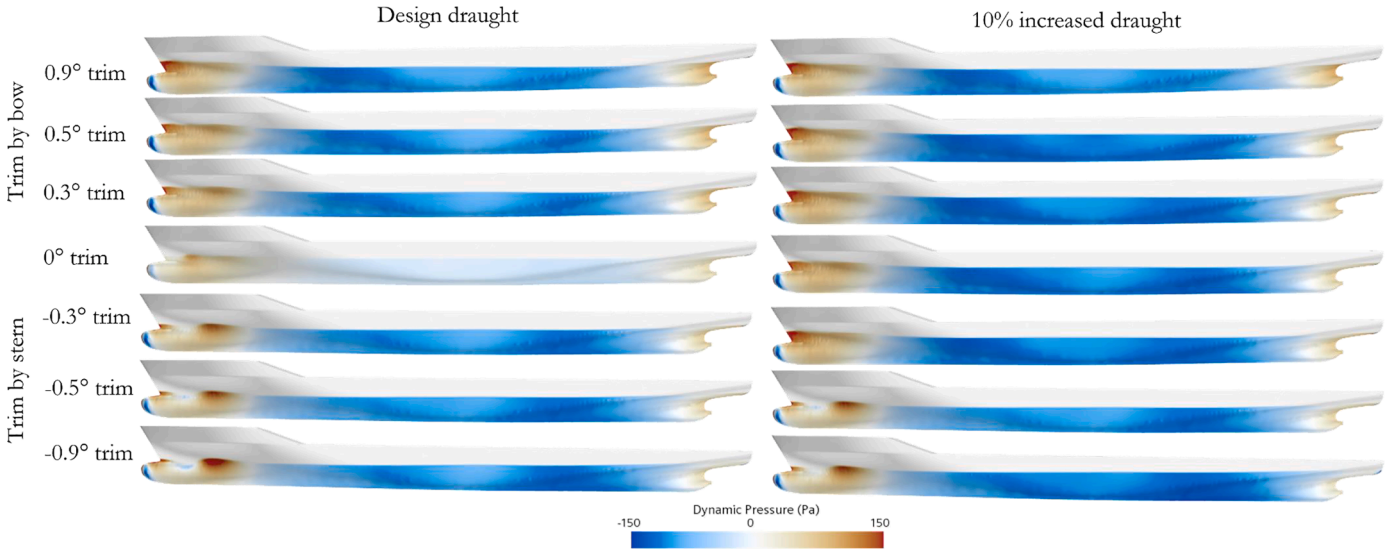

Fig. 11. Dynamic pressure distributions (change with respect to hydrostatic pressure) for the design draught (left) and 10% increased draught (right) for all trim conditions at $F_d = 0.57$.

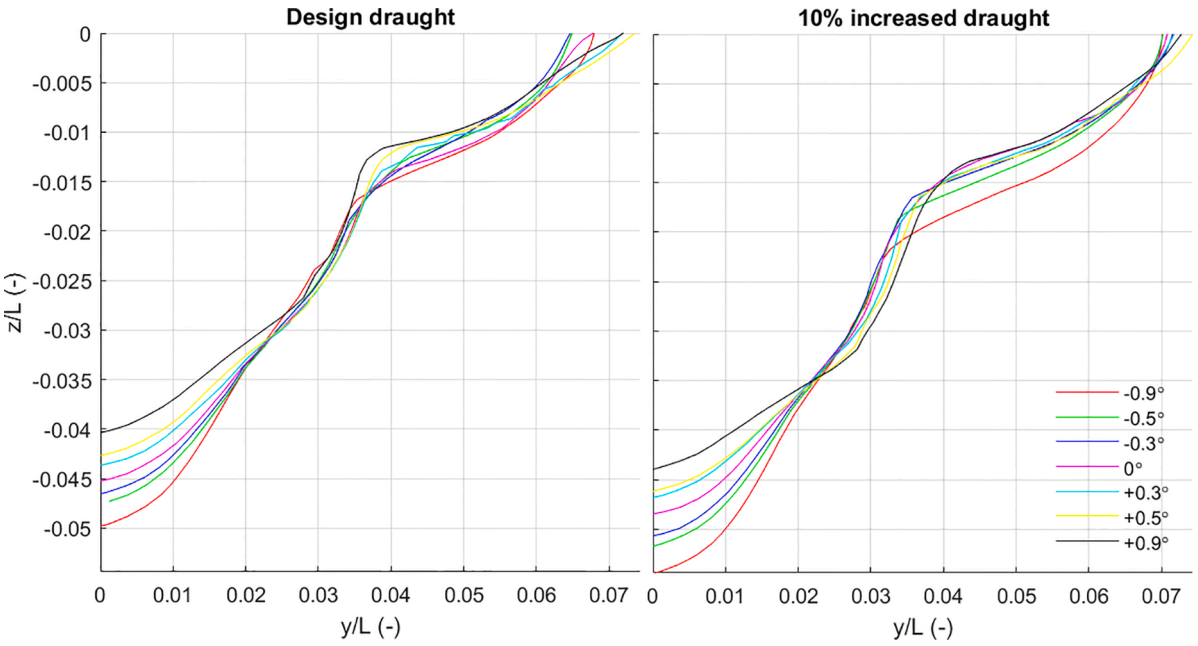

Fig. 12. Boundary layer extents at the aft perpendicular ($x/L = 0$) for the design draught and the 10% increased draught cases for $F_d = 0.57$. Each line represents the location where the flow velocity attains a value equal to 90% of the free stream velocity. Negative trim angles represent trim by stern.

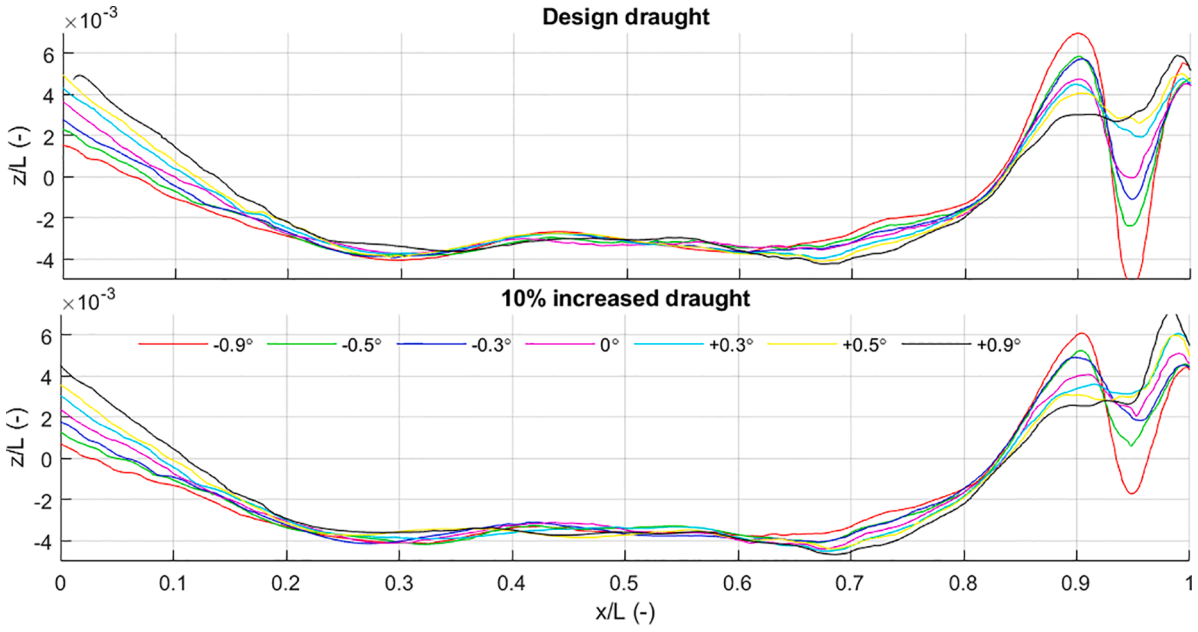

Fig. 13. Wave elevation on the hull for the design draught and the 10% increased draught cases for $F_d = 0.57$.

It is instructive to examine the dimensional values of the resistance components alongside the relative difference of each case with respect to the even keel case. Fig. 8 shows that the pressure resistance increases strongly, by approximately 40% and 70% when the vessel is trimmed by stern ($-0.9°$). This pattern holds true for all speeds, but also, the relative changes are predicted to be to a great extent independent of the draught increase. As evidenced by the changes relative to the even keel condition, the change in the 5% and 10% increase draught are very similar to those predicted for the design draught. The dependence to speed can also be highlighted: the largest increases to stern are found when $F_d = 0.469$.

Clearly, low values of the pressure resistance are more likely to be found when the vessel is trimmed by bow. As mentioned previously, pressure resistance is usually smaller than the frictional component, therefore, the variation of the pressure resistance coefficient must be considered in conjunction with the frictional resistance, which shown in Fig. 9. The frictional resistance coefficients show a different behaviour to C_P. The main cause of variation is the ship speed and draught. This means there is comparatively little change in the path of the smallest C_F predicted by the numerical model. This path is identical for the design draught and the 5% increased draught case, indicating that the least C_F case experiences small changes as a result of the wetted area changes. Additionally, the frictional resistance coefficient is smaller when the vessel is trimmed by stern by $-0.3°$ for the design and 5% increased draught. This explains why the pressure resistance coefficients and the total resistance coefficients do not exhibit the same least resistance cases

as the most favourable. The 10% increased draught case is predicted to have the least frictional resistance contribution in the even keel and -0.5° case depending on the ship speed.

To understand the changes in the frictional resistance better, dimensional equivalents of C_F are given in Fig. 10. The frictional resistance changes proportionately to the trim, driven mostly by changes in the wetted surface area, as mentioned in the literature review. Relative to the even keel condition, the frictional resistance changes considerably less than the pressure resistance, showing a variation in the range approximately ±4.5% as opposed to +70% to −10% as shown in Fig. 8. Nevertheless, friction dominates the total resistance, particularly at low speeds, where the greatest change in pressure resistance is observed. Therefore, a small relative difference in friction stemming from the change in wetted area may counter any changes brought about by modifying the pressure resistance.

To better visualise such changes and explain the relative change in the pressure resistance coefficient, dynamic pressure distributions over the wetted area must be examined. This is depicted in Fig. 11, where the design draught and the 10% increased draught are compared in the case where $\boldsymbol{F_d} = 0.57$.

Fig. 11 demonstrates that the bow wave is split into two components and delayed significantly when the vessel is trimmed by stern. By contrast, the trim by bow cases exhibit a single elevation with a peak near the forward perpendicular. This observation also explains the supressed resistance hump in the cases where the vessel is trimmed by bow. Such humps would be expected when examining the range of speeds included in this study, and is apparent in the cases where the vessel is trimmed by stern. Additionally, a re-examination of Fig. 4 reveals that the resistance hump in the -0.9° cases has switched from $\boldsymbol{F_d} = 0.502$ in the design and 5% increased draught cases to $\boldsymbol{F_d} = 0.496$ in the 10% increased draught case.

The results presented above show that pressure resistance, the normal component of the total, is influenced to a greater extent by variations in trim than frictional resistance. There is therefore a strong case for using potential flow-based methods for such investigations. However, viscous effects should also be taken into account for the following reasons. The stern area of the hull may be subject to strong viscous effects since the boundary layer is thicker than at the bow with consequences for wave making resistance (Song et al., 2019). Since wave making is influenced by these facts, it stands to reason that inviscid approaches may not fully capture the consequences of variations in the trim of a hull. Cuts of the boundary layer at the aft perpendicular are presented in Fig. 12 to investigate the effect of trim on the flow.

Fig. 12 shows that trim has a considerable influence on the flow affected by viscosity in the stern area of a hull. The main disagreements between case studies are concentrated close to the centreline due to the proximity and position of the hull. Increasing the draught causes these disagreements to intensify, which is expected because viscous effects on ship resistance are known to grow with decreasing underkeel clearance (Zeng et al., 2019). In the majority of the y/L range, the $+0.9^{\circ}$ case has the smallest boundary layer, which rises more sharply and further as x/L is increased from the centreline than other cases.

Viscous contributions to resistance are the primary cause of scale effects on ship resistance, it is therefore expected that magnifying the importance of viscosity will lead to greater scale effects. Terziev et al. (2021) and Zeng et al. (2019) explored the influence of shallow water on scale effects confirming that shallow water magnifies scale effects. The results presented herein are therefore expected to suffer scale effects when extrapolated to full-scale, particularly due to changes in the waterline shape. Waterline shapes obtained using the model-scale simulations discussed above are compared in Fig. 13 for the design draught and the case where the draught is increased by 10%. The split in the bow wave elevation identified in Fig. 11 is confirmed, namely, as the vessel is trimmed by stern, the first wave trough at near the bow intensifies considerably when compared to cases where the vessel is trimmed by bow. Additionally, the design draught causes a larger oscillation when the vessel is trimmed by stern than at the 10% increased draught. In all cases, the $+0.9^{\circ}$ case shows the highest bow wave elevation and stern wave elevation. A reduction in the water level at the hull implies the flow is accelerated more than in other cases, causing additional friction and explaining the differences in frictional resistance observed in Fig. 10.

At the vessel's parallel midbody, the wave elevation is largely unaffected by variations in trim. However, near the stern wave elevations split and are arranged in ascending order vertically from -0.9° to $+0.9^{\circ}$ vertically. Increasing the vessel draught causes the spread at the stern (near $x/L = 0$) to be greater: from approximately $2z/L \times 10^{-3}$ to $4z/L \times 10^{-3}$ in the design and 10% increased draught cases, respectively. As discussed previously, the same region experiences the greatest influence of viscosity and will be subject to scale effects. Particular care should therefore be given to reaching conclusions on the optimum trim envelope of a vessel in the absence of full-scale results and the use of inviscid methods.

5. Conclusion and future work

Reynolds averaged Navier-Stokes numerical simulations using the commercial software Star-CCM+, version 14.06.009, were carried out to explore the effect of a ship's trim angle and draught on its resistance in confined waters. To this end, a set of five speeds ($F_d = 0.302 \sim 0.57$), seven trim angles ($\pm 0.9^{\circ}$, $\pm 0.5^{\circ}$, $\pm 0.3^{\circ}$, and 0°), and three ship draughts (design – 0% increase, 5% increase, and 10% increase) were modelled. The first step was to perform a validation and verification study on the level keel case (0° trim, 0% draught increase), for all speeds in the design condition, which resulted in a successful validation of the majority of ship speeds. Validation uncertainties in the range 5.24% and 2.11% were found for $F_d = 0.469$ and $F_d = 0.502$, respectively.

For the examined ship, in the confined water channel investigated, the KCS showed the least resistance when trimmed by bow. However, a strong speed dependence was shown to influence the best trim angle. Changes in draught also contribute to determining the least total resistance coefficient. Similarly to other studies highlighted in the literature review section, the results presented herein show that pressure resistance is considerably more sensitive to changes in the trim than frictional resistance. The former is predicted to increase by up to approximately 70% when the vessel is trimmed by stern and reduce by approximately 15% when trimmed by bow. Conversely, frictional resistance exhibits changes by no more than 5% regardless of the trim condition.

According to the numerical model, increases in the draught of the KCS may incur a hydrodynamic penalty of up to approximately 15.08% for $F_d = 0.469$ when compared to the design draught. However, the vessel trim can compensate this to a large extent. Specifically, the results presented herein showed that in the case of 10% increased draught and $F_d = 0.303$, the total resistance coefficient is 0.87% higher than the design loading condition if the vessel is trimmed by 0.9° (trim by bow). The highest examined speed showed a 0.34% reduction in the total resistance for the same case. This result has implications for the design of vessels, since it points to the possibility of fitting larger, more efficient propellers on deeper draught craft with little downside if the trim is taken into account. Significant changes in boundary layer and wave elevation were shown near the stern. Since the stern area of a hull is where viscous effects are strongest extrapolation to full-scale will incur scale effects which must be taken into account when proving design or operational recommendations. Additionally, care must be taken when providing trim optimisation advise since at some conditions the transom may immerse. Growth in the stern wave height as a result of scale effects may also cause such an effect.

The study can be extended in a number of ways. Two suggestions could be the inclusion of sinkage and trim to model ship squat and its effect on resistance, which was not taken into account in the current model. Similarly, the effects of self-propulsion should be examined,

since a variation in the trim will also impact propeller performance. The study could also be enhanced by employing a typical inland hull, rather than a benchmark geometry. That would however require experimental data at a variety of data points to ensure the computational model is validated against several of the examiend conditions as was done in the present study.

CRediT authorship contribution statement

Ruaraidh Campbell: Conceptualization, Data curation, Formal analysis, Investigation, Methodology, Software, Validation, Visualization, Writing – original draft, Writing – review & editing. **Momchil Terziev:** Conceptualization, Data curation, Formal analysis, Investigation, Methodology, Project administration, Software, Supervision, Validation, Visualization, Writing – original draft, Writing – review & editing. **Tahsin Tezdogan:** Conceptualization, Funding acquisition, Project administration, Resources, Supervision, Validation, Writing – review & editing. **Atilla Incecik:** Conceptualization, Funding acquisition, Project administration, Resources, Supervision, Validation, Writing – review & editing.

Declaration of Competing Interest

The authors declare that they have no known competing financial interests or personal relationships that could have appeared to influence the work reported in this paper.

Acknowledgments

Results were obtained using the ARCHIE-WeSt High Performance Computer (www.archie-west.ac.uk) based at the University of Strathclyde. Figs. 3–10 were produced using MatPlotLib, created by Cobeldick (2021). The underlying data used in the paper is openly available through the University of Strathclyde repository at: 10.15129/3b633085-7d3a-40ef-bf3f-53de0e126076

References

Altosole, M., Figari, M., Ferrari, A., Bruzzone, D., Vernengo, G., 2016. Experimental and numerical investigation of draught and trim effects on the energy efficiency of a displacement mono-hull. In: Proceedings of the International Offshore and Polar Engineering Conference, pp. 857–863.

Andrun, M., Blagojević, B., Bašić, J., 2018. The influence of numerical parameters in the finite-volume method on the Wigley hull resistance. In: . https://doi.org/10.1177/1475090218812956.

ASME (American Society of Mechanical Engineers), 2009. Standard for Verification and Validation in Computational Fluid Dynamics and Heat Transfer. ASME International. ASME V&V 20-2009.

Celik, I.B., Ghia, U., Roache, P.J., Freitas, C., 2008. Procedure for estimation and reporting of uncertainty due to discretization in CFD applications. J. Fluids Eng. 130, 078001 https://doi.org/10.1115/1.2960953.

Chen, J., Yu, C., Shen, L., 2019. Study of trim optimization based on design of experiments and RANS simulation. In: Proceedings of the International Workshop on Ship and Marine Hydrodynamics. Hamburg, Germany, pp. 1–7.

Cobeldick, S., 2021. MatPlotLib Perceptually Uniform Colormaps (https://www.mathworks.com/matlabcentral/fileexchange/62729-matplotlib-perceptually-uniform-colormaps) [WWW Document]. MATLAB Cent. File Exch.

Du, P., Ouahsine, A., Sergent, P., 2017. Influence of the draft to ship dynamics in the virtual tank based on openfoam. In: Proceedings of the International Conference on Computational Methods in Marine Engineering, pp. 996–1003. Mar. 2017 2017-May.

Du, P., Ouahsine, A., Sergent, P., Hu, H., 2020. Resistance and wave characterizations of inland vessels in the fully-confined waterway. Ocean Eng. 210 https://doi.org/10.1016/j.oceaneng.2020.107580.

Duan, W., Zhang, H., Huang, L., Liu, J., Shao, W., Cao, G., Shi, Z., 2019. Numerical simulation of trim optimization on resistance performance based on CFD method. In: Proceedings of the International Conference on Ocean, Offshore, and Arctic Engineering (OMAE), 2, pp. 1–9. https://doi.org/10.1115/OMAE2019-96181.

Elsherbiny, K., Tezdogan, T., Kotb, M., Incecik, A., Day, A.H., 2019a. An experimental investigation of the trim effect on the behaviour of a containership in shallow water. In: Proceedings of the ASME 38th International Conference on Ocean, Offshore and Arctic Engineering. Glasgow, UK. OMAE2019.

Elsherbiny, K., Tezdogan, T., Kotb, M., Incecik, A., Day, S., 2019b. Experimental analysis of the squat of ships advancing through the New Suez Canal. Ocean Eng. 178, 331–344. https://doi.org/10.1016/j.oceaneng.2019.02.078.

Ferziger, J.H., Peric, M., 2002. Computational Methods for Fluid Dynamics. Springer. https://doi.org/10.1016/S0898-1221(03)90046-0.

Iakovatos, M.N., Liarokapis, D.E., Tzabiras, G.D., 2013. Experimental investigation of the trim influence on the resistance characteristics of five ship models. Developments in Maritime Transportation and Exploitation of Sea Resources. CRC Press, Taylor and Francis, pp. 1–1118.

Inland Waterways Association (IWA), 2020. IWA Vision for Sustainable Propulsion on the Inland Waterways. Inland Waterways Association (IWA).

Islam, H., Soares, G., 2019. Effect of trim on container ship resistance at different ship speeds and drafts. Ocean Eng. 183, 106–115. https://doi.org/10.1016/j.oceaneng.2019.03.058.

ITTC, 2017. Quality system manual recommended procedures and guidelines procedure uncertainty analysis in CFD verification and validation.

ITTC, 2014. ITTC – recommended procedures and guidelines - practical guidelines for ship CFD applications. 7.5-03-02-03 (Revision 01). ITTC – Recomm. Proced. Guidel. 19.

ITTC, 2011. Recommended procedures and guidelines: practical guidelines for ship CFD. In: Proceedings of the 26th International Towing Tank Conference.

IWA (Inland Waterways Association), 2020. IWA vision for sustainable propulsion on the inland waterways.

Jones, D.A., Clarke, D.B., 2010. Fluent code simulation of flow around a naval hull: the DTMB 5415. Def. Sci. Technol. Organ. Victoria (Australia), Marit. platforms Div.

Kallinderis, Y., Kontzialis, C., 2009. A priori mesh quality estimation via direct relation between truncation error and mesh distortion. J. Comput. Phys. 228, 881–902. https://doi.org/10.1016/j.jcp.2008.10.023.

Le, T.H., Vu, M.T., Bich, V.N., Phuong, N.K., Ha, N.T.H., Chuan, T.Q., Tu, T.N., 2021. Numerical investigation on the effect of trim on ship resistance by RANSE method. Appl. Ocean Res. 111, 102642 https://doi.org/10.1016/j.apor.2021.102642.

Lv, X., Wu, X., Sun, J., Tu, H., 2013. Trim optimization of ship by a potential-based panel method. Adv. Mech. Eng. 2013 https://doi.org/10.1155/2013/378140.

Lyu, X., Tu, H., Xie, D., Sun, J., 2018. On resistance reduction of a hull by trim optimization. Brodogradnja 69, 1–13. https://doi.org/10.21278/brod69101.

Moustafa, M.M., Yehia, W., Hussein, A.W., 2015. Energy efficient operation of bulk carriers by trim optimization. In: Proceedings of the 18th International Conference on Ships and Shipping Research, pp. 484–493. NAV 2015.

Pacuraru, F., Domnisoru, L., 2017. Numerical investigation of shallow water effect on a barge ship resistance. IOP Conf. Ser. Mater. Sci. Eng. 227 https://doi.org/10.1088/1757-899X/227/1/012088.

Park, H.S., Seo, D.W., Han, K.M., Kim, D.H., Ha, T.B., 2015. A study on resistance performance for various trim conditions and bulb shapes on a container ship under slow steaming. In: Proceedings of the International Conference on Offshore Mechanics and Arctic Engineering OMAE. St John's Newfoundland, Canada, pp. 1–8. https://doi.org/10.1115/OMAE201541782.

Perera, L.P., Mo, B., Kristjánsson, L.A., 2015. Identification of optimal trim configurations to improve energy efficiency in ships. IFAC-PapersOnLine 28, 267–272. 10.1016/j.ifacol.2015.10.291.

Phillips, T., 2014. Residual-based discretization error estimation for computational fluid dynamics 148.

Richardson, L.F., 1927. Deferred approach to the limit. Trans. R. Soc. Lond. Ser. A 226, 299–361.

Roache, P.J., 1998. Validation and verification in computational science and engineering. Hermosa Albuquerque, NM.

Rotteveel, E., Hekkenberg, R., van der Ploeg, A., 2017. Inland ship stern optimization in shallow water. Ocean Eng. 141, 555–569. https://doi.org/10.1016/j.oceaneng.2017.06.028.

Roy, C.J., Blottner, F.G., 2006. Review and assessment of turbulence models for hypersonic flows: 2D/asymmetric cases. In: Proceedings of the 44th AIAA Aerospace Sciences Meeting and Exhibit. https://doi.org/10.2514/6.2006-713.

Sherbaz, S., Duan, W., 2014. Ship trim optimization: assessment of influence of trim on resistance of MOERI container ship. Sci. World J. 603695 https://doi.org/10.1155/2014/603695, 2014.

Shivachev, E., Khorasanchi, M., Day, A.H., 2017. Trim influence on KRISO container ship (KCS); an experimental and numerical study. In: Proceedings of the ASME 36th International Conference on Ocean, Offshore and Arctic Engineering, pp. 1–7. https://doi.org/10.1115/OMAE2017-61860.

Siemens, 2018. Star-CCM+ User Guide version 13.04.

Sogihara, N., Tsujimoto, M., Fukasawa, R., Ohba, H., 2018. Investigation on trim optimization to enhance the propulsive performance of fine ships. J. Jpn. Soc. Nav. Archit. Ocean Eng. 27, 15–22. https://doi.org/10.2534/jjasnaoe.27.15.

Song, S., Demirel, Y.K., Atlar, M., 2019. An investigation into the effect of biofouling on the ship hydrodynamic characteristics using CFD. Ocean Eng. 175, 122–137. https://doi.org/10.1016/j.oceaneng.2019.01.056.

Sun, J., Tu, H., Chen, Y., Xie, D., Zhou, J., 2016. A study on trim optimization for a container ship based on effects due to resistance. J. Ship Res. 60, 30–47. https://doi.org/10.5957/JOSR.60.1.150022.

Terziev, M., Tezdogan, T., Incecik, A., 2021. A numerical assessment of the scale effects of a ship advancing through restricted waters. Ocean Eng. 229, 108972 https://doi.org/10.1016/j.oceaneng.2021.108972.

Terziev, M., Tezdogan, T., Incecik, A., 2020a. Application of eddy-viscosity turbulence models to problems in ship hydrodynamics. Ships Offshore Struct. 15 https://doi.org/10.1080/17445302.2019.1661625.

Terziev, M., Tezdogan, T., Incecik, A., 2020b. A posteriori error and uncertainty estimation in computational ship hydrodynamics. Ocean Eng. 208, 107434 https://doi.org/10.1016/j.oceaneng.2020.107434.

Tezdogan, T., Incecik, A., Turan, O., 2016. A numerical investigation of the squat and resistance of ships advancing through a canal using CFD. J. Mar. Sci. Technol. 21, 86–101. https://doi.org/10.1007/s00773-015-0334-1.

The European Commission, 2020. Assessment of the potential of maritime and inland ports and inland waterways and of related policy measures, including industrial policy measures. 10.2832/03796.

Tuck, E.O., 1978. Hydrodynamic problems of ships in restricted waters. Annu. Rev. Fluid Mech. 10, 33–46.

Wu, D., Wang, J., Wan, D., 2021. Delayed detached eddy simulation method for breaking bow waves of a surface combatant model with different trim angle. Ocean Eng. 242, 110177 https://doi.org/10.1016/j.oceaneng.2021.110177.

Yan, G.K.K., Ollivier-Gooch, C., 2017. Applications of the unsteady error transport equation on unstructured meshes. In: Proceedings of the 23rd AIAA Computational Fluid Dynamics Conference. Denvel, Colorado. https://doi.org/10.2514/6.2017-4112, 2017.

Zeng, Q., Hekkenberg, R., Thill, C., 2019. On the viscous resistance of ships sailing in shallow water. Ocean Eng. 190, 106434 https://doi.org/10.1016/j.oceaneng.2019.106434.